Nano Research 2015, 8(6): 2092–2101
DOI 10.1007/s12274-015-0720-3
Research Article

ISSN 1998-0124
CN 11-5974/O4

Hierarchical TiO_2 photocatalysts with a one-dimensional heterojunction for improved photocatalytic activities

Yingjuan Xie[1,2], Xiao Zhang[1,3], Peijun Ma[1,4], Zhijiao Wu[1], and Lingyu Piao[1] (✉)

[1] *CAS Key Laboratory for Standardization and Measurement for Nanotechnology, National Center for Nanoscience and Technology, Beijing 100190, China*
[2] *Department of Chemistry, University of Chinese Academy of Sciences, Beijing 100049, China*
[3] *Institute of Optoelectronics Technology, Beijing Jiaotong University, Beijing 100044, China*
[4] *College of Chemical Engineering, Beijing University of Chemical Technology, Beijing 100029, China*

Received: 12 November 2014
Revised: 7 January 2015
Accepted: 8 January 2015

KEYWORDS

one-dimensional heterojunction,
TiO_2,
photocatalytic activity

ABSTRACT

Hierarchical TiO_2 photocatalysts with a one-dimensional heterojunction were synthesized via a facile template-free hydrothermal method. The TiO_2 photocatalysts were flower-like microspheres with a 3 μm diameter. The base structure of the flower-like microspheres was a uniform nanowire with a 10 nm diameter. Anatase films were evenly coated onto the surface of the rutile TiO_2 nanowires to form a one-dimensional core–shell base structure. This kind of one-dimensional heterojunction is conducive to the separation of charge carriers. In addition, the hierarchical TiO_2 microspheres possessed a good mesoporous structure with a high specific surface area of 260 m^2/g. Thus, the light scattering and utilization efficiency were improved in this structure. The photocatalysts exhibited better performance in both photocatalytic oxidation and reduction reactions. Moreover, the novel TiO_2 photocatalysts displayed excellent stability in these reactions. This kind of hierarchical TiO_2 structure has never been reported in the literature. The hierarchical structure and one-dimensional heterojunction were vital to the increase in quantum efficiency. Therefore, these hierarchical TiO_2 photocatalysts have potential applications in the environmental and energy fields, such as in photocatalytic degradation, hydrogen production, Li-ion batteries, and dye-sensitized solar cells.

1 Introduction

Titanium dioxide (TiO_2), which is an important material among metal oxide semiconductors, has attracted a great deal of attention [1–3] due to its high photocatalytic activity, low cost, and nontoxic properties in photocatalytic [4–6] and photovoltaic [7–9] applications. Anatase and rutile are the most commonly used crystal forms of TiO_2 [10–12]. Many studies have shown that anatase is more active than rutile in photocatalytic

---

Address correspondence to piaoly@nanoctr.cn

reactions [13, 14]. When compared with pure-phase TiO_2 nanomaterials, anatase/rutile mixed-phase TiO_2 exhibits a higher photocatalytic activity because of the promoted vectorial charge transfer and carrier separation rate at the interface of the two phases [15–19].

Three-dimensional hierarchical structures have attracted interest in recent years due to their potential applications in photocatalytic degradation reactions, dye-sensitized solar cells, Li-ion batteries, and water splitting [20–31]. More active sites are provided by hierarchical structures with a considerably large specific surface area. In addition, the light utilization efficiency and structural stability is enhanced in hierarchical photocatalysts [32–41]. Considering the advantages of a mixed-phase crystal structure, some efforts were made in the fabrication of hierarchical TiO_2 with mixed-phase structures [42–45]. For example, Shi et al. have prepared a hierarchical mixed-phase TiO_2 photocatalyst with anatase nanocrystals wrapped onto the surface of rutile spheres [42]. Ye et al. have synthesized hierarchical TiO_2 nanotube arrays composed of anatase TiO_2 nanotubes with small rutile nanocrystals on the tube walls [43]. All of the prepared photocatalysts showed higher activity than pure-phase TiO_2 photocatalysts. However, a high charge recombination exists within nanoparticles due to the trapping and scattering of electrons at grain boundaries. Moreover, inefficient light scattering of the above mixed-phase hierarchical TiO_2 structures limited the improvement of light utilization efficiency. To overcome this obstacle, we have designed a kind of hierarchical TiO_2 structure with the following properties: (1) It has a hierarchical flower-like microsphere structure; (2) the base structure of the hierarchical TiO_2 photocatalysts is a uniform nanowire with a 10 nm diameter; and (3) the base structure is a mixed-phase heterojunction with anatase films evenly coated onto the surface of rutile nanowires to form a one-dimensional core–shell structure. The one-dimensional TiO_2 base structure resulted in less recombination of the photogenerated electrons and holes.

Here, we obtained hierarchical TiO_2 microspheres (HTM) with a one-dimensional heterojunction structure for the first time. The hierarchical TiO_2 photocatalysts were formed by the self-assembly of one-dimensional nanowires, and the nanowire base structures were composed of mixed phases (anatase and rutile). The anatase was evenly coated onto the surface of the rutile TiO_2 nanowires to form a one-dimensional core–shell structure. The one-dimensional heterojunction was more conducive to the separation of charge carriers and was important for the increase of quantum efficiency. The photocatalytic activities of the hierarchical TiO_2 photocatalysts with a mixed-phase structure were evaluated by both photocatalytic oxidation and reduction reactions.

2 Experimental

2.1 Synthesis of mixed-phase TiO_2 powder (m-TiO_2)

In a typical procedure, 2 mL of tetrabutyl titanate (TBOT) was added directly into a mixed solution of 50 mL of ethanol and 82 mL of deionized water at ambient temperature. After magnetic stirring for 10 min, 4.73 mL of hydrochloric acid (HCl, 1 M) was added to the solution. The resulting solution was heated to 100 °C for 22 h. Subsequently, the solution was allowed to cool down to ambient temperature. The products were collected using centrifugation, washed with ethanol and deionized water, and then vacuum freeze-dried to obtain a homogeneous mixed-phase TiO_2 powder (Fig. S1 in the Electronic Supplementary Material (ESM)).

2.2 Synthesis of hierarchical TiO_2 with one-dimensional heterojunction structures

The prepared mixed-phase TiO_2 powders (0.01 g) were dispersed into 60 mL of sodium hydroxide solution (NaOH, 7 M) in a 100 mL Teflon-lined autoclave. The hydrothermal reaction was performed at 150 °C for 5 h. The white precipitate was collected using centrifugation, washed with deionized water and HNO_3 (0.1 M) several times, and then air dried at 80 °C.

2.3 Characterization

The morphologies of the samples were examined using field emission scanning electron microscopy (FE-SEM, Hitachi S-4800) and transmission electron microscopy (TEM, Tecnai G2 20 S-TWIN). The selected area electron diffraction (SAED) patterns were obtained at an accelerating voltage of 200 kV. The X-ray powder diffraction (XRD, Bruker D8 Advance) patterns were obtained using a diffractometer with Cu Kα radiation (λ = 1.54056 Å). The Raman spectra were recorded on a Renishaw inVia Raman microspectrometer using a laser excitation wavelength of 633 nm. X-ray photoelectron spectroscopy (XPS, Escalab 250Xi) was performed using Mg Kα X-rays as the excitation source. UV–Vis diffuse reflectance spectra (DRS) of the samples were collected using a UV–Vis spectrometer (Hitachi U-3900) with an integrating sphere at ambient temperature. Nitrogen adsorption-desorption isotherms (ASAP 2020, Micromeritics Instruments) were collected at 77 K. Thermogravimetric analyses (TGA, PerkinElmer Diamond TG) were also performed. Room-temperature photoluminescence (PL) spectra of the samples were recorded using a fluorescence spectrophotometer (PerkinElmer LS 55, excitation at 270 nm).

2.4 Photocatalytic degradation of methylene blue (MB)

The photodegradation experiments were performed in a quartz reactor containing 100 mL of 10 mg/L methylene blue (MB) solution and 0.02 g of catalyst. The mixture was continuously stirred in the dark for 1 h to reach the adsorption–desorption equilibrium between the catalyst and MB before irradiation. Then the mixture was irradiated with a Xe lamp (with a wavelength peak at 365 nm, and approximately 10 $mW\cdot cm^{-2}$). An aliquot of the solution was removed every 5 min and centrifuged to remove the solid catalyst. The concentration of MB was then determined from the absorbance at 665 nm using a UV–Visible spectrometer (Hitachi U-3900). The pH of the MB solution varied between 7.0–7.7 during the degradation process. The experiments were repeated five times under the same conditions.

2.5 Water splitting reactions

Photocatalytic H_2 production experiments were conducted in a sealed vessel connected to a glass-enclosed gas circulation system (LABSOLAR-H_2IIIAG, PerfectLight, China). 0.15 wt% of Pt was loaded on TiO_2 as a co-catalyst by photoreduction of chloroplatinic acid ($H_2PtCl_6\cdot 6H_2O$) using methanol as a scavenger. In a typical experiment, 0.01 g of a sample loaded with Pt was suspended in 100 mL of 50% aqueous methanol solution under magnetic stirring, and the reaction temperature was maintained at 5 °C using a recirculation cooler. A 300 W Xe lamp was used in the photocatalytic reactions, and the distance between the lamp and the vessel was 16 cm. The amount of H_2 evolved was determined using a gas chromatograph (TechcoMp, GC 7900) with a thermal conductivity detector (TCD).

3 Results and discussion

3.1 Morphological and structural characterization of HTM

The morphologies and structures of the HTM samples were characterized using FESEM and TEM.

Figure 1(a) displays a high uniformity of three-dimensional flower-like architectures. The assemblies were in the range of 3–3.5 μm in diameter. The SEM (Figs. 1(b) and 1(c)) and TEM images (Figs. 1(d) and 1(e)) showed that the microspheres were composed of serried nanowires, which were 10–15 nm in diameter. An HRTEM image of a typical nanowire is depicted in Fig. 1(f). The lattice fringes and the distribution of the two phases were clearly visible. The lattice fringes with inter-plane spacings of 0.353 nm and 0.650 nm were attributed to the spacing of the (101) plane of the anatase phase and the double spacing of the (110) plane of the rutile phase, respectively [46, 47]. Thus, the prepared HTM consisted of a structure with an anatase film forming a shell around a core of rutile nanowires. The interfaces between the anatase and rutile (the red dotted lines in Fig. 1(f)) were clear, which indicated the formation of one-dimensional heterojunctions. The region between the two red dotted lines was indexed to rutile and the outer region was indexed to anatase. The SAED image (the inset of Fig. 1(e)) proved the existence of a polycrystalline mixed-phase, because the diffraction rings could be assigned to the (101) and (200) planes of anatase TiO_2, and the (110) and (002) planes of rutile TiO_2, respectively.

The crystal phase of the HTM was characterized using XRD and Raman technologies, which confirmed the coexistence of anatase and rutile. As can be seen in Fig. 2(a), the 2θ values at 25.28, 37.8, and 48.06° were

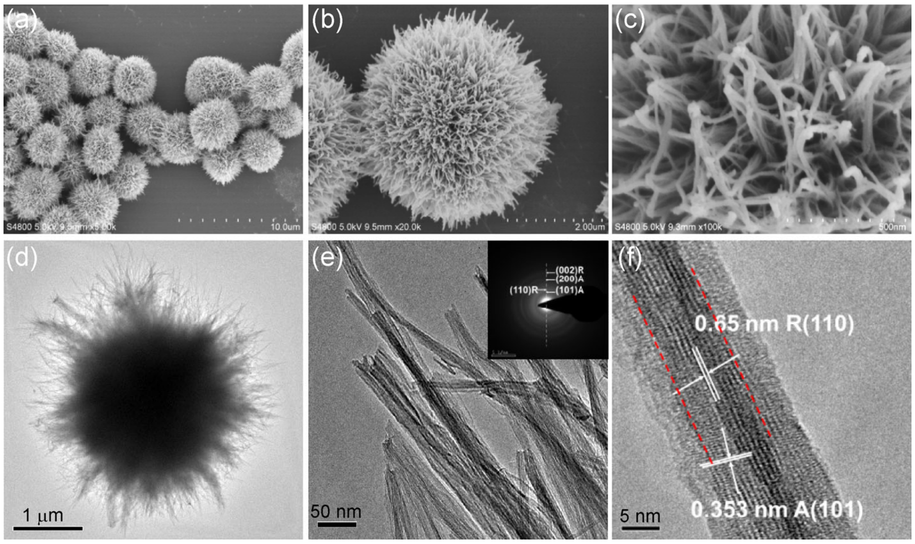

Figure 1 SEM images ((a), (b), and (c)), TEM images ((d) and (e)), an HRTEM image (f), and the SAED pattern (inset of (e)) of the prepared HTM.

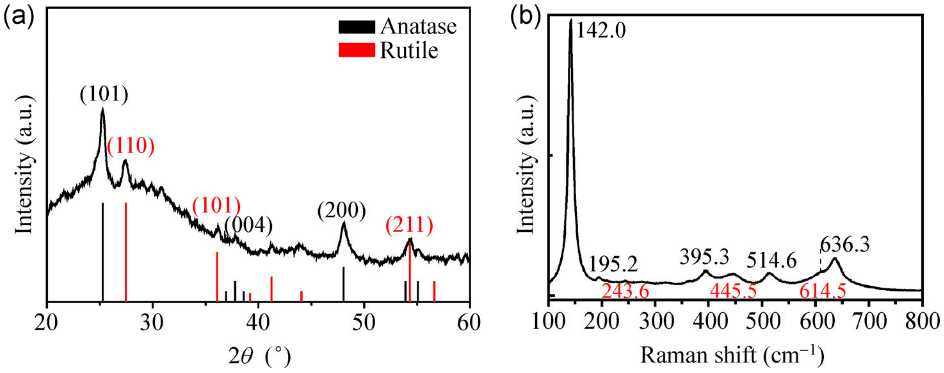

Figure 2 The XRD pattern (a), and Raman spectrum (b) of the prepared HTM.

assigned to the (101), (004), and (200) crystal planes of anatase TiO_2 respectively. The 27.4, 36.22, 41.24, and 54.34° peaks were assigned to (110), (101), (111), and (211) crystal planes of rutile TiO_2, respectively. All of the peaks were indexed to anatase (JCPDS card No. 21-1272) or rutile (JCPDS card No. 21-1276) phases. In addition, the weight fraction of the anatase phase (WA), which was calculated using Eq. (S1) in the ESM was 64.9 wt%. Figure 2(b) shows the Raman spectrum of the prepared HTMs, which exhibited more evidence of the mixed phases. The characteristic Raman modes at 142.0 cm^{-1} (E_g), 195.2 cm^{-1} (E_g), 395.3 cm^{-1} (B_{1g}), 514.6 cm^{-1} (A_{1g}), and 636.3 cm^{-1} (E_g) were assigned to the Raman active modes of anatase, whereas the characteristic Raman modes at 243.6 cm^{-1} (two-phonon scattering), 445.5 cm^{-1} (E_g), and 614.5 cm^{-1} (A_{1g}) were assigned to those of rutile [18]. These results were in accordance with the XRD patterns. The results from the HRTEM, SAED, XRD, and Raman spectra indicated that the HTM samples consisted of mixed phases, which included anatase and rutile. Furthermore, the anatase film was uniformly coated on the outside of the rutile nanowires and the mixed-phase formed a one-dimensional core–shell structure. Figure 3 presents the nitrogen adsorption–desorption isotherms and pore size distribution curve of the HTM. The isotherm was a typical type IV according to the IUPAC classification. The pore distribution range was from 1–10 nm, and the HTM primarily contained mesopores with diameters of 2.1 nm, 3.6 nm, and 4.9 nm. The diameter of MB molecules is approximately 1.1 nm, which is smaller than the mesopores of the HTM; therefore, the transfer and diffusion of dyes during the photodegradation reaction could be promoted to enhance

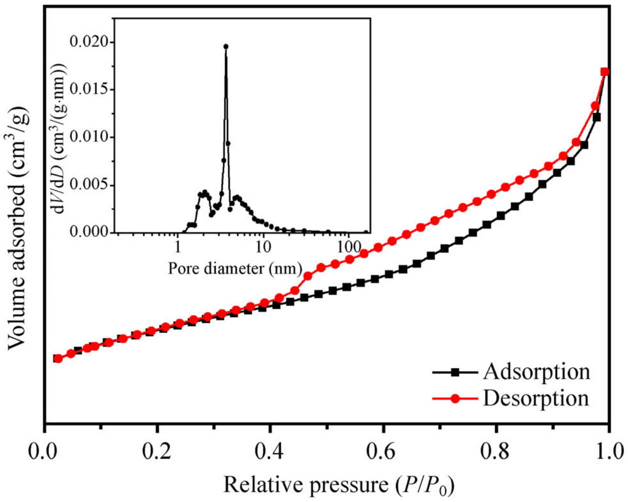

Figure 3 Nitrogen adsorption-desorption isotherms and the pore size distribution curve (inset).

the reaction rate [42]. This is also suitable for phenol (0.7 nm) and other molecules whose diameters are less than the size of the mesopores. The measurement showed that the BET surface area of the HTM was approximately 260 $m^2 \cdot g^{-1}$. This was very favorable for its application in a photocatalytic reaction. To determine the thermal stability of the HTM, a TG analysis was performed (Fig. S2 in the ESM). From Fig. S2, a total weight loss of 4% was observed in the temperature range of 50–400 °C, and there was no further weight loss after 400 °C.

The 4% weight loss was mainly attributed to the evaporation of adsorbed H_2O and CO_2. Therefore, we concluded that the HTM was very clean and stable after calcination.

Further evidence for the mixed-phase of the hierarchical TiO_2 photocatalysts comes from the XPS analysis (Fig. 4). A TiO_2 nanowire (TiO_2–NW) is the base structure of the hierarchical anatase TiO_2 (Fig. S3 in the ESM). Photoelectron peaks corresponding to Ti and O were observed in the XPS survey spectra (Fig. 4(a)) for the HTM, P25, and TiO_2–NW. A C emission peak could be observed in the samples of the HTM, P25, and TiO_2–NW, which might have resulted from the transfer process of the sample into the UHV chamber. All of the products exhibited two Ti 2p peaks as shown in Fig. 4(b), which were assigned to the Ti^{4+} spectra of bulk TiO_2. The binding energy of Ti $2p_{3/2}$ for the HTM and P25 was located at 458.18 eV, which was about 0.17 eV lower than that of the TiO_2–NW (458.33 eV). These results further confirmed the composition of the HTM and P25 (which were mixed-phase TiO_2) was different from that of the TiO_2–NW (which was only anatase).

3.2 Optical properties of HTM

The optical properties of the HTM, TiO_2–NW, and P25 were investigated using UV–Vis diffuse reflectance spectra and photoluminescence spectra (Fig. 5).

After calculating, the E_g values were approximately 3.36 eV (inset of Fig. 5(a)) and 3.19 eV for the HTM and P25, respectively. Figure 5(a) shows that a blue shift of E_g occurred in the HTM samples when compared with TiO_2–NW and P25, which revealed that the band gap was extended. The band gap extension was related to the size of the nanowire base structures due to the quantum size and mixed-phase effects of semiconductors. The HTM has a low reflectivity in the visible wavelength range of 400–600 nm, which indicated that the HTM has a better light-scattering

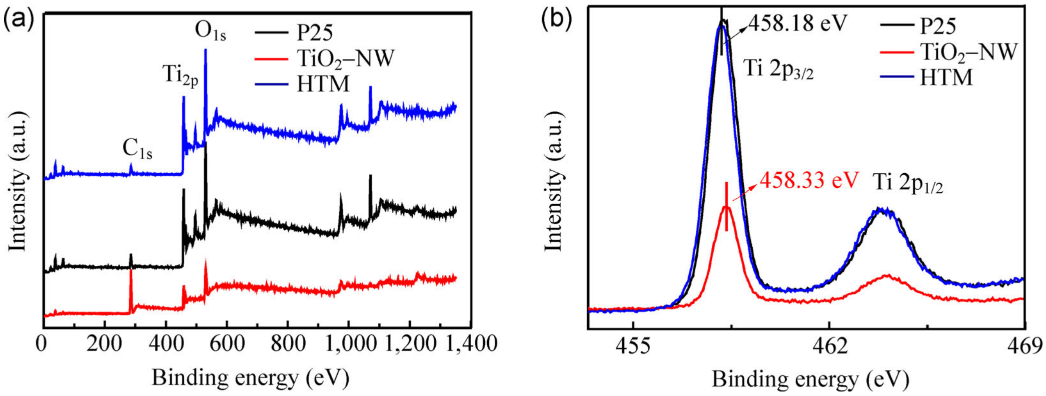

Figure 4 (a) XPS full survey spectrum of the HTM, P25, and TiO_2-NW; and (b) the Ti 2p spectra.

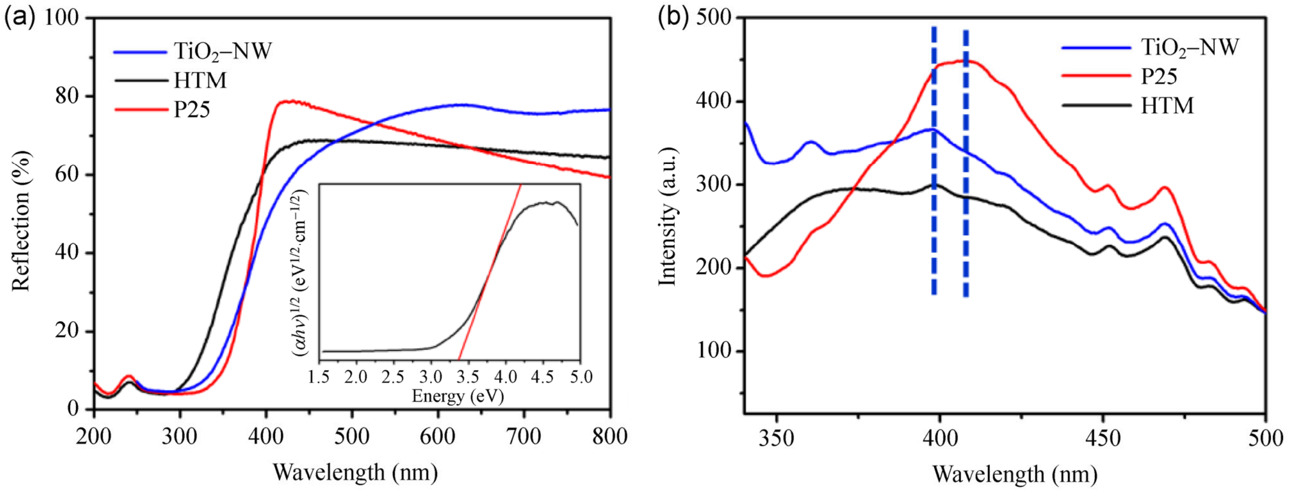

Figure 5 (a) UV–Vis DRS spectra of samples and the plot of $(\alpha h\nu)^{1/2}$ vs. energy ($h\nu$) of the HTM (inset); (b) the PL spectra of the samples.

ability than that of P25. This was because the HTM could allow multiple reflections of the light between 400–600 nm.

PL spectra are often used to investigate electron-hole recombination after irradiation. From Fig. 5(b), five peaks at approximately 371, 452, 468, 483, and 493 nm were divided into two main regions (340–420 nm and 450–550 nm). The former was assigned to the emission of the band gap transition, whereas the latter was assigned to the emission of the charge transfer transition. The charge transfer transition was caused by the recombination of photoexcited electrons with holes occupying the oxygen vacancies in the TiO_2 [18, 48–51]. We note that an emission at 371 nm for the HTM samples was blue shifted when compared with P25 (414 nm), which was attributed to the larger value of E_g. The PL intensities for the prepared HTM at the other four positions were lower than those of TiO_2–NW and P25. This indicated that the HTM samples had a lower rate of electron-hole recombination, and consequently, a much higher photocatalytic activity.

3.3 Photocatalytic Activity of HTM

The photocatalytic activity of HTM was evaluated using photo-oxidation and reduction reactions. The photo-oxidation reaction was performed using the degradation of an MB solution under UV light irradiation. Figure S4 in the ESM shows the UV–Vis absorption spectra of a MB solution after different irradiation times under different photocatalysts. The results indicated that the photodegradation of the dye was complete. No intermediate products were detected. Figure 6(a) shows the values of photocatalytic activity for the HTM, P25, and TiO_2–NW [52] and Fig. S5 in the ESM shows the condition of MB self degradation under UV light irradation.

We observed that the HTM and TiO_2–NW exhibited higher activity than that of P25. The photodegradation reaction of MB obeyed first-order kinetics. By plotting $\ln(C_0/C)$ as a function of time, the reaction rate constant k was obtained. The values of k and the specific activity (k/S_{BET}, the ratio of the reaction rate constant k and the surface area S_{BET}) are shown in Table S1 in the ESM. The order of the specific activities was HTM > TiO_2–NW > P25. The light harvesting of the hierarchical photocatalysts (HTM and TiO_2–NW) was improved greatly when compared with particles (P25) due to the multiple reflection effect. The band gaps of the HTM and TiO_2–NW were wider than that of P25 because of the smaller size of the base structures (quantum size effect). Therefore, the oxidation capacity of the HTM was the strongest among the catalysts. The specific activity of the HTM was better than that of TiO_2–NW, which was attributed to the heterogeneous structure of the HTM, which included increased separation efficiency of the photogenerated electrons and holes.

In addition to photocatalytic efficiency, the recyclability and stability of the hierarchical TiO_2 photocatalysts are essential factors for practical applications. Figure 6(b) shows the degradation half-life and eighty percent-life

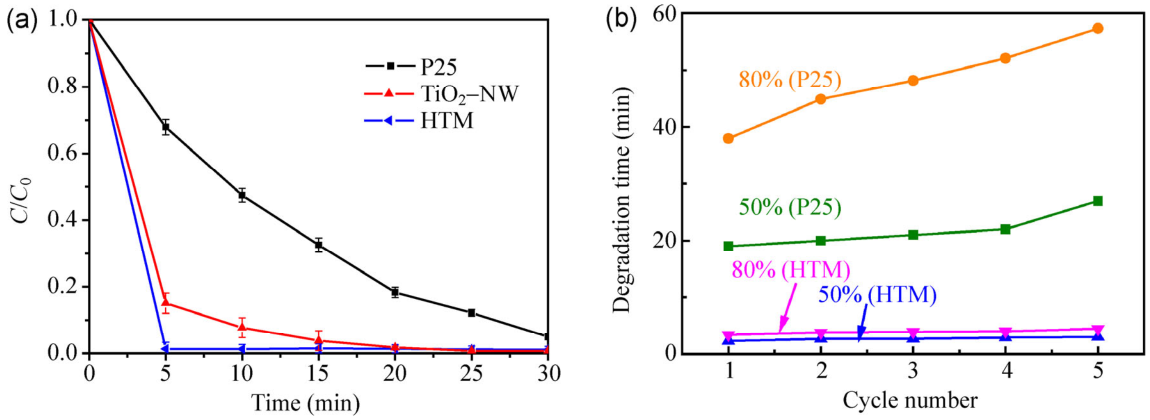

Figure 6 (a) Degradation curves; and (b) degradation half-life and eighty percent-life of MB (C_0 = 10 mg/L) solution under UV light irradiation by commercial Degussa P25, TiO_2–NW, and the HTM.

of MB on the HTM and P25 as a function of cycle number. The degradation time of MB on P25 increased with increasing cycle numbers, which demonstrated its poor stability. However, the HTM could be effectively recycled at least five times without a significant increase in the degradation time, which indicated that it had high repeatability and stability. Furthermore, the crystalline phases of the HTM were stable without any observed changes after the photocatalytic reaction (Fig. S6 in the ESM). When compared with the hierarchical TiO_2 with one-dimensional nanowires as base structures, nanoparticles (such as P25) tended to aggregate in the suspension during photocatalytic cycles, which led to a rapid decline of their photocatalytic activity [53].

To evaluate the photo-reduction activity of the HTM, a series of experiments for hydrogen production through water splitting were performed. Figure 7 shows the rate of H_2 evolution of the HTM, TiO_2–NW, and sample 64.9% A/R. The sample 64.9% A/R was composed of mixed-phase anatase and rutile nanoparticles (Fig. S7 in the ESM), which contained 64.9% anatase. The amount of H_2 generated from the 0.15% Pt/HTM was more than twice the amount from the 0.15% Pt/TiO_2–NW and 0.15% Pt/A/R, which was mainly due to the larger band gap of the HTM.

The corresponding scheme of photo-oxidation and photo-reduction processes is shown in Fig. 8. The sample 64.9% A/R is particle in shape. The loaded Pt influenced the reactive surface area of the 64.9% A/R catalyst. The effect was more obvious than that on the HTM and TiO_2–NW. However, the loaded amount of

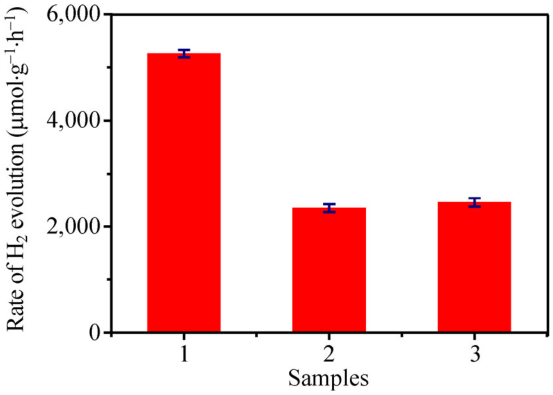

Figure 7 Hydrogen evolved per gram of photocatalysts per hour under UV light irradiation in aqueous solution.

Pt was only 0.15%, and the effect on their photoreduction was not a key factor because the Pt was a co-catalyst. The photoreactivity mainly depended upon the properties of the TiO_2. The HTM, which has a larger band gap, has a more negative potential of conduction band and a longer electron lifetime when compared to TiO_2–NW and 64.9% A/R. The high photocatalytic activity of the HTM was also attributed to the transfer of electrons from the anatase conduction band to the lower rutile conduction band. The transfer could effectively separate the photogenerated electrons and holes, which led to a higher H_2 production activity. The Pt nanoparticles were effective electron acceptors that facilitated the electron capture. The photogenerated electrons transferred from the anatase to the rutile, and finally accumulated onto the Pt nanoparticles to enhance the photo-reduction activity. Simultaneously, the holes in the valence band of the anatase could produce hydroxyl radicals for the

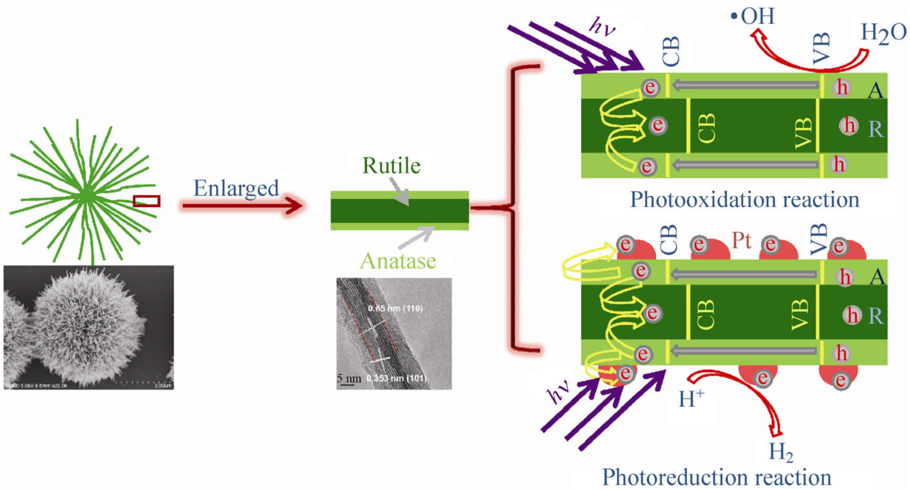

Figure 8 Scheme of the HTM to enhance the photooxidation and photoreduction reaction.

oxidative decomposition of methanol, dyes, or other pollutants (in other application fields).

4 Conclusions

To improve the quantum efficiency and stability of TiO_2 photocatalysts, a hierarchical TiO_2 with one-dimensional heterojunction structures was prepared for the first time. The TiO_2 photocatalysts consisted of flower-like microspheres with a 3 μm diameter. The base structure of the flower-like microspheres was a uniform nanowire with a 10 nm diameter. The nanowire was a one-dimensional core–shell structure with anatase films evenly coated onto the surface of rutile. The content of anatase in the photocatalyst was approximately 64.9%. The one-dimensional heterojunctions were more conducive to the separation of charge carriers and important in the improvement of quantum efficiency. This novel photocatalyst had a mesoporous structure with a high specific surface area. The mass transfer and diffusion of dyes during the photodegradation reactions could be promoted.

The results of the photocatalytic oxidation indicated that the photocatalyst had better performance and stability than P25. In addition, the photocatalyst was extremely active in the production of hydrogen. With these merits, this hierarchical TiO_2 having one-dimensional heterojunction structures has potential applications in environmental and energy fields such as in photocatalytic degradation, hydrogen production, Li-ion batteries, and dye-sensitized solar cells. The combination of a variety of advantages in a photocatalyst is important in the structural and functional design of materials.

Acknowledgements

The authors gratefully acknowledge the financial support from the Ministry of Science and Technology of China (No. 2011FY130104), and the National Basic Research Program of China (973 Program, No. 2011CB932802). We are grateful to the support from CAS Key Laboratory for Standardization and Measurement for Nanotechnology.

Electronic Supplementary Material: Supplementary material is available in the online version of this article at http://dx.dio.org/10.1007/s12274-015-0720-3.

References

[1] Fujishima, A.; Zhang, X. T.; Tryk, D. A. TiO_2 photocatalysis and related surface phenomena. *Surf. Sci. Rep*. **2008**, *63*, 515–582.

[2] Chen, X. B.; Mao, S. S. Synthesis of titanium dioxide (TiO_2) nanomaterials. *J. Nanosci. Nanotechno*. **2006**, *6*, 906–925.

[3] Chen, X. B.; Mao, S. S. Titanium dioxide nanomaterials synthesis properties modifications and applications. *Chem. Rev*. **2007**, *107*, 2891–2959.

[4] Xiong, Z. G.; Zhao, X. S. Nitrogen-doped titanate-anatase core–shell nanobelts with exposed {101} anatase facets and

enhanced visible light photocatalytic activity. *J. Am. Chem. Soc*. **2012**, *134*, 5754–5757.

[5] Zuo, F.; Bozhilov, K.; Dillon, R. J.; Wang, L.; Smith, P.; Zhao, X.; Bardeen, C.; Feng, P. Y. Active facets on titanium(III)-doped TiO_2: An effective strategy to improve the visible-light photocatalytic activity. *Angew. Chem. Int. Ed*. **2012**, *51*, 6223–6226.

[6] Hu, Y. H. A highly efficient photocatalyst-hydrogenated black TiO_2 for the photocatalytic splitting of water. *Angew. Chem. Int. Ed*. **2012**, *51*, 12410–12412.

[7] Yang, L. J.; Leung, W. W.-F. Electrospun TiO_2 nanorods with carbon nanotubes for efficient electron collection in dye-sensitized solar cells. *Adv. Mater*. **2013**, *25*, 1792–1795.

[8] Wang, Z. Y.; Lou, X. W. TiO_2 nanocages: Fast synthesis, interior functionalization and improved lithium storage properties. *Adv. Mater*. **2012**, *24*, 4124–4129.

[9] Kamat, P. V. TiO_2 nanostructures: Recent physical chemistry advances. *J. Phys. Chem. C* **2012**, *116*, 11849–11851.

[10] Li, J.-G.; Ishigaki, T.; Sun, X. D. Anatase, brookite, and rutile nanocrystals via redox reactions under mild hydrothermal conditions: Phase-selective synthesis and physicochemical properties. *J. Phys. Chem. C* **2007**, *111*, 4969–4976.

[11] Holmberg, J. P.; Johnson, A.-C.; Bergenholtz, J.; Abbas, Z.; Ahlberg, E. Near room temperature synthesis of monodisperse TiO_2 nanoparticles: Growth mechanism. *J. Phys. Chem. C* **2013**, *117*, 5453–5461.

[12] Nonoyama, T.; Kinoshita, T.; Higuchi, M.; Nagata, K.; Tanaka, M.; Sato, K.; Kato, K. TiO_2 synthesis inspired by biomineralization: Control of morphology, crystal phase, and light-use efficiency in a single process. *J. Am. Chem. Soc*. **2012**, *134*, 8841–8847.

[13] Wu, C. Y.; Yue, Y. H.; Deng, X. Y.; Hua,W. M.; Gao, Z. Investigation on the synergetic effect between anatase and rutile nanoparticles in gas-phase photocatalytic oxidations. *Catal. Today* **2004**, *93–95*, 863–869.

[14] Zachariah, A.; Baiju, K. V.; Shukla, S.; Deepa, K. S.; James, J.; Warrier, K. G. K. Synergistic effect in photocatalysis as observed for mixed-phase nanocrystalline titania processed via sol-gel solvent mixing and calcination. *J. Phys. Chem. C* **2008**, *112*, 11345–11356.

[15] Liu, Z. Y.; Zhang X. T.; Nishimoto, S.; Jin, M.; Tryk, D. A.; Murakami, T.; Fujishima, A. Anatase TiO_2 nanoparticles on rutile TiO_2 nanorods: A heterogeneous nanostructure via layer-by-layer assembly. *Langmuir* **2007**, *23*, 10916–10919.

[16] Su, R.; Bechstein, R.; So, L.; Vang, R. T.; Sillassen, M.; Esbjornsson, B.; Palmqvist, A.; Besenbacher, F. How the anatase-to-rutile ratio influences the photoreactivity of TiO_2. *J. Phys. Chem. C* **2011**, *115*, 24287–24292.

[17] van der Meulen, T.; Mattson, A.; Österlund, L. A comparative study of the photocatalytic oxidation of propane on anatase, rutile, and mixed-phase anatase–rutile TiO_2 nanoparticles: Role of surface intermediates. *J. Catal*. 2007, *251*, 131–144.

[18] Su, W. G.; Zhang, J.; Feng, Z. C.; Chen, T.; Ying, P. L.; Li, C. Surface phases of TiO_2 nanoparticles studied by UV Raman spectroscopy and FT-IR spectroscopy. *J. Phys. Chem. C* **2008**, *112*, 7710–7716.

[19] Zhang, J.; Xu, Q.; Feng, Z. C.; Li, M. J.; Li, C. Importance of the relationship between surface phases and photocatalytic activity of TiO_2. *Angew. Chem. Int. Ed*. **2008**, *47*, 1766–1769.

[20] Wu, H. B.; Hng, H. H.; Lou, X. W. Direct synthesis of anatase TiO_2 nanowires with enhanced photocatalytic activity. *Adv. Mater*. **2012**, *24*, 2567–2571.

[21] Feng, X. J.; Zhai, J.; Jiang, L. The fabrication and switchable super hydrophobicity of TiO_2 nanorod films. *Angew. Chem. Int. Ed*. **2005**, *44*, 5115–5118.

[22] Zhao, B.; Chen, F.; Huang, Q. W.; Zhang, J. L. Brookite TiO_2 nanoflowers. *Chem. Commun*. **2009**, *34*, 5115–5117.

[23] Sun, Z. Q.; Kim, J. H.; Zhao, Y.; Bijarbooneh, F.; Malgras, V.; Lee, Y.; Kang, Y. M.; Dou, S. X. Rational design of 3D dendritic TiO_2 nanostructures with favorable architectures. *J. Am. Chem. Soc*. **2011**, *133*, 19314–19317.

[24] Tang, Y. X.; Wee, P. X.; Lai, Y. K.; Wang, X. P.; Gong, D. G.; Kanhere, P. D.; Lim, T.-T.; Dong, Z. L.; Chen, Z. Hierarchical TiO_2 nanoflakes and nanoparticles hybrid structure for improved photocatalytic activity. *J. Phys. Chem. C* **2012**, *116*, 2772–2780.

[25] Ye, M. D.; Liu, H.-Y.; Lin, C. J.; Lin, Z. Q. Hierarchical rutile TiO_2 flower cluster-based high efficiency dye-sensitized solar cells via direct hydrothermal growth on conducting substrates. *Small* **2013**, *9*, 312–321.

[26] Bian, Z. F.; Zhu, J.; Wang, J. G.; Xiao, S. X.; Nuckolls, C.; Li, H. X. Multitemplates for the hierarchical synthesis of diverse inorganic materials. *J. Am. Chem. Soc*. **2012**, *134*, 2325–2331.

[27] Chen, J. S.; Tan, Y. L.; Li, C. M.; Cheah, Y. L.; Luan, D. Y.; Madhavi, S.; Boey, F. Y. C.; Archer, L. A.; Lou, X. W. Constructing hierarchical spheres from large ultrathin anatase TiO_2 nanosheets with nearly 100% exposed (001) facets for fast reversible lithium storage. *J. Am. Chem. Soc*. **2010**, *132*, 6124–6130.

[28] Wang, W.; Ni, Y.; Lu, C. H.; Xu, Z. Z. Direct solvethermal growth of hierarchical porous TiO_2 nanosheets with high photocatalytic activity. *Mater. Lett*. **2013**, *111*, 161–164.

[29] Cheng, P. F.; Du, S. S.; Cai, Y. X.; Liu, F. M.; Sun, P.; Zheng, J.; Lu, G. Y. Tripartite layered photoanode from hierarchical anatase TiO_2 urchin-like spheres and P25: A candidate for enhanced efficiency dye sensitized solar cells. *J. Phys. Chem. C* **2013**, *117*, 24150–24156.

[30] Yang, M.-H.; Chen, P.-C.; Tsai, M.-C.; Chen, T.-T.; Chang, I.-C.; Chiu, H.-T.; Lee, C.-Y. Anatase and brookite TiO_2 with various morphologies and their proposed building block. *Crystengcomm* **2014**, *16*, 441–447.

[31] Tan, X. H.; Qiang, P. F.; Zhang, D. D.; Cai, X.; Tan, S. Z.; Liu, P. Y.; Mai, W. J. Three-level hierarchical TiO_2 nanostructure based high efficiency dye-sensitized solar cells. *Crystengcomm* **2014**, *16*, 1020–1025.

[32] Liu, M.; Piao, L. Y.; Wang, W. J. Fabrication and characteristics of three-dimensional flower-like titanate nanostructures. *J. Nanosci. Nanotechno. Lett.* **2010**, *10*, 7469–7472.

[33] Ge, M.; Li, J. W.; Liu, L.; Zhou, Z. Template-free synthesis and photocatalytic application of rutile TiO_2 hierarchical nanostructures. *Ind. Eng. Chem. Res.* **2011**, *50*, 6681–6687.

[34] Bai, H. W.; Liu, Z. Y.; Sun, D. D. Hierarchically multifunctional TiO_2 nano-thorn membrane for water purification. *Chem. Commun.* **2010**, *46*, 6542–6544.

[35] Sinha, A. K.; Jana, S.; Pande, S.; Sarkar, S.; Pradhan, M.; Basu, M.; Saha, S.; Pal, A.; Pal, T. New hydrothermal process for hierarchical TiO_2 nanostructures. *Crystengcomm* **2009**, *11*, 1210–1212.

[36] Wu, D. P.; Zhu, F.; Li, J. M.; Dong, H.; Li, Q.; Jiang, K.; Xu, D. S. Monodisperse TiO_2 hierarchical hollow spheres assembled by nanospindles for dye-sensitized solar cells. *J. Mater. Chem.* **2012**, *22*, 11665–11671.

[37] Kondalkar,V. V.; Mali, S. S.; Mane, R. M.; Dandge, P. B.; Choudhury, S.; Hong, C. K.; Patil, P. S.; Patil, S. R.; Kim, J. H.; Bhosale, P. N. Photoelectrocatalysis of cefotaxime using nanostructured TiO_2 photoanode: Identification of the degradation products and determination of the toxicity level. *Ind. Eng. Chem. Res.* **2014**, *53*, 18152–18162.

[38] Patil, P. B.; Mali, S. S.; Kondalkar,V. V.; Pawar, N. B.; Khot, K. V.; Hong, C. K.; Patil, P. S.; Bhosale, P. N. Single step hydrothermal synthesis of hierarchical TiO_2 microflowers with radially assembled nanorods for enhanced photovoltaic performance. *RSC Adv.* **2014**, *4*, 47278–47286.

[39] Ong, W.-J.; Tan, L.-L.; Chai, S.-P.; Yong S.-T.; Mohamed, A. R. Self-assembly of nitrogen-doped TiO_2 with exposed {001} facets on a graphene scaffold as photo-active hybrid nanostructures for reduction of carbon dioxide to methane. *Nano Res.* **2014**, *7*, 1528–1547.

[40] Zhou, W.; Li, T.; Wang, J. Q.; Qu, Y.; Pan, K.; Xie, Y.; Tian, G. H.; Wang, L.; Ren, Z. Y.; Jiang, B. J.; et al. Composites of small Ag clusters confined in the channels of well-ordered mesoporous anatase TiO_2 and their excellent solar-light-driven photocatalytic performance. *Nano Res.* **2014**, *7*, 731–742.

[41] Song, H.; Jo, K.; Jung, B. Y.; Jung, G. Y. Fabrication of periodically aligned vertical single-crystalline anatase TiO_2 nanotubes with perfect hexagonal open-ends using chemical capping materials. *Nano Res.* **2014**, *7*, 104–109.

[42] Shi, F. Z.; Li, Y. G.; Zhang, Q. H.; Wang, H. Z. Preparation of core/shell structured rutile/anatase photocatalyst via vapor phase hydrolysis and its photocatalytic degradation of phenol and methylene blue. *J. Am. Ceram. Soc.* **2012**, *95*, 1927–1932.

[43] Ye, M. D.; Zheng, D. J; Lv, M. Q.; Chen, C.; Lin, C. J.; Lin, Z. Q. Hierarchically structured nanotubes for highly efficient dye-sensitized solar cells. *Adv. Mater.* **2013**, *25*, 3039–3044.

[44] Sun, C. H.; Wang, N. X.; Zhou, S. Y.; Hu, X. J.; Zhou, S. Y.; Chen, P. Preparation of self-supporting hierarchical nanostructured anatase/rutile composite TiO_2 film. *Chem. Commun.* **2008**, *28*, 3293–3295.

[45] Hsu, Y.-C.; Lin, H.-C.; Chen, C.-H.; Liao, Y.-T.; Yang, C.-M. Nonaqueous seeded growth of flower-like mixed-phase titania nanostructures for photocatalytic applications. *J. Solid State Chem.* **2010**, *183*, 1917–1924.

[46] Yu, X.; Xu, H. M.; Xin, L.; Wang, X. Y.; Liu, Y.; Zhou, X.; Li, B. J.; Zhao, W. X.; Shen, H. Synergistic assembly of nanoparticle aggregates and texture nanosheets into hierarchical TiO_2 core–shell structures for enhanced light harvesting in dye-sensitized solar cells. *J. Mater. Chem. A* **2013**, *1*, 6175–6182.

[47] Xu, F.; Zhang, X. Y.; Wu, Y.; Wu, D. P.; Gao, Z. Y.; Jiang, K. Facile synthesis of TiO_2 hierarchical microspheres assembled by ultrathin nanosheets for dye-sensitized solar cells. *J. Alloy. Compd.* **2013**, *574*, 227–232.

[48] Cong, Y.; Zhang, J. L.; Chen, F.; Anpo, M. Synthesis and characterization of nitrogen-doped TiO_2 nanophotocatalyst with high visible light activity. *J. Phys. Chem. C* **2007**, *111*, 6976–6982.

[49] Shi, J. Y.; Chen, J.; Feng, Z. C.; Chen, T.; Lian, Y. X.; Wang, X. L.; Li, C. Photoluminescence characteristics of TiO_2 and their relationship to the photoassisted reaction of water/methanol mixture. *J. Phys. Chem. C* **2007**, *111*, 693–699.

[50] Zhang, J. L.; Hu, Y.; Matsuoka, M.; Yamashita, H.; Minagawa, M.; Hidaka, H.; Anpo, M. Relationship between the local structures of titanium oxide photocatalysts and their reactivities in the decomposition of NO. *J. Phys. Chem. B* **2001**, *105*, 8395–8398.

[51] Nair, R. G.; Paul, S.; Samdarshi, S. K. High UV/visible light activity of mixed phase titania: A generic mechanism. *Sol. Energ. Mat. Sol. C* **2011**, *95*, 1901–1907.

[52] Xie, Y. J.; Wu, Z. J.; Wu, Q.; Liu, M.; Piao, L. Y. Effect of different base structures on the performance of the hierarchical TiO_2 photocatalysts. *Catal. Today* **2014**, *225*, 74–79.

[53] Bao, N.; Li, Y.; Wei, Z. T.; Yin, G. B.; Niu, J. J. Adsorption of dyes on hierarchical mesoporous TiO_2 fibers and its enhanced photocatalytic properties. *J. Phys. Chem. C* **2011**, *115*, 5708–5719.